Heinrich Söding
Institute of Fluid Dynamics and Ship Theory,
Hamburg University of Technology,
Schwarzenbergstrasse 95C,
Hamburg 21073, Germany
e-mail: h.soeding@tuhh.de

Vladimir Shigunov[1]
DNV GL,
Brooktorkai 18,
Hamburg 20457, Germany
e-mail: vladimir.shigunov@dnvgl.com

Thomas E. Schellin
DNV GL,
Brooktorkai 18,
Hamburg 20457, Germany

Ould el Moctar
DNV GL,
Brooktorkai 18,
Hamburg 20457, Germany

A Rankine Panel Method for Added Resistance of Ships in Waves

A new Rankine panel method and an extended Reynolds-Averaged Navier–Stokes (RANS) solver were employed to predict added resistance in head waves at different Froude numbers of a Wigley hull, a large tanker, and a modern containership. The frequency domain panel method, using Rankine sources as basic flow potentials, accounts for the interaction of the linear periodic wave-induced flow with the nonlinear steady flow caused by the ship's forward speed in calm water, including nonlinear free surface conditions and dynamic squat. Added resistance in waves is obtained by the pressure integration method. The time domain RANS solver, based on a finite volume method, is extended to solve the nonlinear equations of the rigid body six-degrees-of-freedom ship motions. The favorable comparison of the panel and RANS predictions demonstrated that the Rankine method is suitable to efficiently obtain reliable predictions of added resistance of ships in waves. Comparable model test predictions correlated less favorably, although the overall agreement was felt to be acceptable, considering the difficulties associated with the procedures to obtain accurate measurements. [DOI: 10.1115/1.4026847]

Introduction

The design of cargo and passenger ships is usually performed on the basis of powering requirements in calm water without considering the actual operating conditions; the effect of the seaway is included using an experience-based allowance on the required power called the sea margin [1]. This practice can lead to either unnecessary excessive power reserves or to underpowered ships that cannot sail against wind and waves in heavy weather [2]. Because of the increased concern with fuel consumption, a reliable prediction of the power increase in waves becomes increasingly important for both ship designers (selection of the engine and propulsion system) and operators (prediction of the service speed and the associated fuel consumption along with the selection of speed and course). This issue is important for regulatory bodies, not only regarding the required redundancy to ensure maneuverability and course keeping in adverse environments, but also regarding the assumed ship speed in waves as a prerequisite for a global strength analysis of the ship's hull girder.

The advance speed in the seaway is defined by the involuntary speed loss (typically in a small to moderate seaway) and voluntary speed reduction (more relevant in heavy to extreme seaways). The involuntary speed loss is caused by both the increased required power and the reduced available power in adverse conditions. The reduction of the available power occurs due to engine overload and the decreased propulsion efficiency due to ship motions and waves, while the increase in the required power is mainly attributable to added resistance in waves and wind, i.e., the mean horizontal force against the average direction of ship movement. In addition to this direct resistance component, waves and wind also induce a time-averaged side force and yaw moment, causing the ship to sail at a certain drift and rudder angle, thereby further increasing the resistance and the required power.

In order to reduce slamming, deck wetness, damage to the cargo or ship structure, or adverse effects on the passengers and crew, the ship master may have to decrease speed or change course or both. This leads to the speed reduction referred to as voluntary. In heavy to extreme seaways, voluntary speed reduction is usually more relevant; this situation may, however, change for under-powered ships.

For the prediction of the power increase in a realistic seaway, the usual approach relies on the application of linear spectral analysis, based on measured responses in towing or self-propulsion model tests in regular (usually head) waves and, additionally, tests in calm water (resistance and self-propulsion tests and open-water propeller tests) to derive the calm-water resistance, thrust deduction factor, wake fraction, and open-water propeller curves [1].

Model test methods use either self-propelled or towed models. The former method ensures a minimum distortion of model motions by the carriage; however, the influence of motions and waves on the thrust deduction factor (required to estimate the added resistance) remains an uncertain factor. Methods with towed models either restrain the model's surge motion [3] or use springs that connect the model to the towing carriage [4,5]. Restraining the surge motion may disturb the heave and pitch motions and, thus, influence the added resistance. The arrangement with springs appears more appropriate; however, the model setup should ensure that the springs do not contribute to the heave and pitch motions. Additionally, springs introduce additional low frequency oscillations in the longitudinal direction, which should be taken into account. Another difficulty in the experimental definition of added resistance in waves is that the added resistance (average force over time) is small compared to the amplitude of the oscillations of the longitudinal force (including Froude–Krylov, radiation, and diffraction parts). Thus, errors in the measurement and averaging of these forces in time might be comparable to, or even exceed, the average force itself. Finally, added resistance is sensitive to the quality of wave generation and wave measurement, especially in short waves, because, unlike the usual linear reactions, added resistance depends on wave amplitude squared.

Computational fluid dynamics (CFD) methods based on the numerical solution of RANS or Euler equations demonstrated their ability to provide results of comparable or superior accuracy to model test measurements in many problems of ship

[1]Corresponding author.

Contributed by the Ocean, Offshore, and Arctic Engineering Division of ASME for publication in the Journal of Offshore Mechanics and Arctic Engineering. Manuscript received September 4, 2012; final manuscript received February 7, 2014; published online April 1, 2014. Assoc. Editor: Dominique Roddier.

hydrodynamics [6,7], but their applications to added resistance predictions are still rare [2,8,9]. Although such methods might, in principle, directly address the problem of power increase in irregular waves (if combined with an engine model), both long waves (and the corresponding large ship motions) and short waves (which contribute to the added resistance through diffraction) have to be simultaneously resolved, which significantly increases the required grid size and computational time. Therefore, the application of CFD methods to the added resistance problem is thus far limited to regular wave situations in a restricted range of wave frequencies.

The question of the required grid density to accurately resolve added resistance with CFD methods should be addressed. Such methods provide the total resistance, including added resistance due to the waves and calm-water contribution (consisting of viscous and wave generation parts); the latter has to be calculated in a separate simulation on the same grid as used for the prediction of the total resistance and subtracted from the total resistance. To accurately compute the calm-water resistance, very fine grids are required, resolving the turbulent boundary layer on the hull and the steady wave system, while, as experience showed (see, e.g., Ref. [9]), much coarser grids are sufficient for the resolution of incoming waves and ship motions that are relevant for added resistance (surge, pitch, and heave). A question arises as to whether such coarser 'seakeeping' grids are sufficient for the calculation of the added resistance in waves. Two types of such grids were tested in Ref. [8] for the calculation of the added resistance in waves: fine grids suitable for the calculation of calm-water resistance and coarser grids optimized to resolve the incoming waves and ship motions; the calm-water contribution (different for different grid types) was separately calculated for both grid types and subtracted from the corresponding total resistance. The predictions of ship motions and added resistance in waves compare favorably between these grid types; see, e.g., Fig. 3, which suggests that added resistance in waves can be computed on coarse grids optimized for seakeeping computations. The calm-water resistance needs to be separately computed on the same grid and subtracted from the average total resistance in order to obtain the value of the added resistance. If, however, an accurate prediction of the total resistance in waves is also required, the calm-water resistance needs to be computed on a sufficiently fine grid and added to the wave-induced added resistance.

Because CFD methods are still too computationally intensive to account for the large number of required parameter variations, potential flow methods are likely to be widely used to predict the added resistance in waves at an early design stage. Linear frequency-domain potential methods have thus far been most popular to calculate added resistance. Although forces averaged over an encounter period depend upon the second (and higher) power on wave amplitude, they can be approximately estimated from quadratic (and higher-order) combinations of the linear potentials of fluid motions. Such methods can quickly produce results for a large number of conditions, albeit neglecting part of the nonlinear effects. One of these effects is the hull shape above the calm-water waterline: model tests and full-scale measurements [10] and numerical simulations [11] showed that the bow sharpness above the calm-water waterline influences the added resistance of bulk carriers and very large crude carriers (VLCCs) high in head waves. While potential theory-based time-domain simulations can account for this effect, they become unstable when periodic motions incur periodic wave breaking. Another nonlinear effect is viscosity: although viscosity has little effect on those ship motions that contribute most to added resistance, i.e., heave and pitch [12], ship motions in waves can lead to periodic vortex separation from appendages, e.g., bilge keels, or from the ship hull itself, which induces, on average, a nonzero horizontal force. Thus, CFD simulations are necessary to predict some components of the added resistance in waves.

The increased resistance in waves is usually assumed to be caused by the (a) wave radiation due to ship motions, and (b) diffraction of incident waves by the ship hull. In head waves the greatest contribution to wave radiation stems from heave and pitch motions. The radiation-induced added resistance is large when ship motions are large, i.e., in relatively long waves. The diffraction of incident waves produces a diffraction-induced component of added resistance, which depends weakly on the wave frequency and thus becomes the dominating component in shorter waves, where ship motions are small.

Perhaps the first theoretical approach to calculate the added resistance in waves was introduced by Maruo [13] and further elaborated in Refs. [14–16]; this approach is based on the consideration of the diffracted and radiated wave energy and momentum flux at infinity. The radiated wave energy method [17], in a similar way, equates the energy contained in the waves radiated from the ship per encounter wave period to the work of the added resistance per encounter period. This approach thus resolves only the radiated energy caused by the ship's motions, while it accounts for the diffraction in short waves by an empirical formula.

Another possibility for calculating the added resistance is to average over the wave encounter period the second-order contributions to the force acting in the average direction of the ship movement from the wetted on the average and periodically emerging and submerging parts of the hull surface. Perhaps the first description of such an approach, usually referred to as the integrated pressure method, appeared in Ref. [18].

Although these methods should provide the same results if all second-order terms are consistently considered, this is usually not the case, because different simplifications and different numerical implementations are used. Reference [19] documents a favorable agreement between the results based on Maruo's theory [13] and the results from direct pressure integrations for a Series 60 hull, a Wigley III hull, and a submerged spheroid at zero forward speed in head waves.

In short waves, added resistance is difficult to accurately predict. In Ref. [20], an analytical asymptotic formula for added resistance in short waves is derived, taking into account only the diffraction part of the added resistance and the interaction between the diffraction of the waves and the steady flow around the ship, which is frequently used together with other methods in order to approximate the high-frequency part of the added resistance.

Rankine source methods, introduced into seakeeping problems, perhaps first by Yeung [21], have been used for added resistance computations in Refs. [19,22–24]. Here, a newly developed three-dimensional Rankine panel method of Söding [25] (also see Ref. [26] for a more detailed description of the method) is applied. This method accounts for the interaction of the linear periodic wave-induced flow with the nonlinear steady flow caused by the ship's forward speed in calm water, taking into account the nonlinear free surface conditions and dynamic squat. The added resistance in waves is obtained by pressure integration.

The code 'GL Rankine' is used here to compute the added resistance in head waves at different Froude numbers of a Wigley III hull, a large tanker, and a modern containership. For the container ship and the Wigley hull, the RANS solvers COMET [27] and Star-CCM+ [28], respectively, were employed to obtain comparative predictions of added resistance in waves. The results were also compared to model test measurements.

Added Resistance With the Rankine Method

Linear seakeeping analysis describes the ship response (motions, sectional forces, and moments, hull pressures, etc.) as harmonic in time, neglecting effects that depend nonlinearly upon the wave height. Time averages of the linear responses are zero. However, waves also generate forces and moments that are nonzero when averaged over a wave encounter period. The lowest nonzero order of these forces and moments is two, i.e., for a small wave amplitude they are proportional to ζ_a^2, which is the wave amplitude squared. Of most practical importance are the sway

force and the yaw moment and the longitudinal force (called added resistance). Usually, a complete analysis of the potential flow up to second-order is not performed, because it is complicated and introduces problems with the accuracy of the numerical approximations. More importantly, only a few terms dominate the result; these terms can be estimated using only the linear flow solution.

The method used for the linear analysis was developed in Ref. [25]; a more detailed description can be found in Ref. [26]. Here, only a brief description is given for convenience. The flow potential $\phi(\mathbf{x},t)$, depending on location $\mathbf{x}$ (the coordinate system is moving forward with the average ship speed U in the x-direction), and time t is composed of three parts, including the potential of the parallel incident flow, the potential of the steady disturbance of the incident flow caused by the hull, and the potential of the time-periodic flow oscillating at the encounter frequency ω_e

$$\phi(\mathbf{x},t) = -Ux + \phi_0(\mathbf{x}) + \mathrm{Re}\left[\hat{\phi}(\mathbf{x})e^{i\omega_e t}\right] \tag{1}$$

where $\hat{}$ above a symbol denotes the complex amplitude. All known linear seakeeping Rankine source methods use this equation; Söding [25] developed another subdivision, following the proposal by Hachmann [29], who employed it in a strip method

$$\phi(\mathbf{x},t) = -Ux + \phi_0(\underline{\mathbf{x}}) + \mathrm{Re}\left[\hat{\phi}(\underline{\mathbf{x}})e^{i\omega_e t}\right] \tag{2}$$

where $\underline{\mathbf{x}}$ designates the same location as $\mathbf{x}$, however, expressed in a coordinate system fixed to the ship's hull. The specialty of this method is that the steady flow field follows not only the average forward motion of the ship, but also participates in the periodic flow motion. This, together with the interaction between the stationary disturbance potential ϕ_0 with the periodic first-order potential $\phi_1(\underline{\mathbf{x}},t) = \mathrm{Re}[\hat{\phi}(\underline{\mathbf{x}})e^{i\omega_e t}]$, proved to yield a higher accuracy at high forward speeds.

The difference between the vectors $\mathbf{x}$ in the inertial coordinates and $\underline{\mathbf{x}}$ in the body-fixed coordinates is described with the following second-order equation:

$$\mathbf{x} = \underline{\mathbf{x}} + \mathbf{v}_1 + \mathbf{v}_2 \tag{3}$$

where

$$\mathbf{v}_1 = \mathbf{u} + \alpha \times \underline{\mathbf{x}}$$

and

$$\mathbf{v}_2 = \alpha \times (\alpha \times \underline{\mathbf{x}})/2$$

represent the first- and second-order terms, respectively. Here, $\mathbf{u}$ denotes the displacement of the ship-fixed coordinate origin and α is the rotation of the hull. Expressions similar to Eq. (3) are used for normal vectors, forces, etc.

The second-order force is separated into two main contributions, namely, the pressure force $\mathbf{F}_A^{(2)}$ acting on the hull up to the average waterline (expressed in hull-bound coordinates) and the force $\mathbf{F}_B^{(2)}$ caused by the variation of hull submergence. Force $\mathbf{F}_A^{(2)}$ is a sum of three contributions

$$\mathbf{F}_A^{(2)} = \sum_{\text{panels}} (\underbrace{\underline{p}_0\mathbf{f}_2}_{B} + \underbrace{\underline{p}_1\mathbf{f}_1}_{A} + \underbrace{\underline{p}_2\mathbf{f}_0}_{C}) \tag{4}$$

where the indices 0, 1, and 2 designate the order of pressure $\underline{p}$ in the hull-fixed coordinates and of the area vectors $\mathbf{f}$ of the panels in inertial coordinates. The area vectors $\mathbf{f}$ are normal vectors on the hull panels, pointing into the hull, with magnitudes equal to the panel areas. The area vectors in the inertial coordinates on the order of 0, 1, and 2 are defined, respectively, as

$$\mathbf{f}_0 = \underline{\mathbf{f}}$$
$$\mathbf{f}_1 = \alpha \times \underline{\mathbf{f}}$$

and

$$\mathbf{f}_2 = \alpha \times (\alpha \times \underline{\mathbf{f}})/2$$

Pressures on the order of 0, 1, and 2 are defined as

$$\underline{\hat{p}}_0/\rho = -gz \tag{5}$$

$$p_1/\rho = \mathrm{Re}\left(\hat{p}_1 e^{-i\omega_e t}/\rho\right) \tag{6}$$

with

$$\underline{\hat{p}}_1/\rho = -(\nabla\phi_0 - \mathbf{U})\left(\nabla\hat{\phi} + \hat{\boldsymbol{\alpha}} \times \nabla\phi_0\right) - i\omega_e\left(\hat{\phi} - \hat{\mathbf{v}}_1\nabla\phi_0\right) - g\hat{v}_{1z}$$

and

$$\begin{aligned}\underline{p}_2/\rho = {} & \dot{\mathbf{v}}_2\nabla\phi_0 + \dot{\mathbf{v}}_1(\nabla\nabla\phi_0)\mathbf{v}_1 + (\underline{\alpha}\times\mathbf{v}_1)\nabla\phi_0 - \nabla\dot{\phi}_1\mathbf{v}_1 \\ & - g\mathbf{v}_{2z} - (\nabla\phi_1 - \nabla\phi_0\times\alpha)^2/2 - (\nabla\phi_0 - \mathbf{U})\cdot[(\mathbf{v}_1\nabla\nabla\phi_0)\times\alpha \\ & + (\mathbf{v}_1\times\alpha)\nabla\nabla\phi_0 + \mathbf{v}_1\nabla\nabla\phi_1 - \mathbf{v}_1(\nabla\nabla\nabla\phi_0)\mathbf{v}_1]\end{aligned} \tag{7}$$

respectively. The symbols $\nabla\nabla$ in the expressions $\nabla\nabla\phi_0$ denote an outer product, producing a matrix when applied to a scalar, and the symbol $\nabla\nabla\nabla$ in the expression $\nabla\nabla\nabla\phi_0$ also denotes an outer product, producing a tensor of third-order when applied to a scalar.

The three terms in parentheses in Eq. (4) each consist of two harmonically oscillating factors contributing to the second-order force. These time-harmonic factors are denoted as $a = \mathrm{Re}(\hat{a}e^{i\omega_e t})$ and $b = \mathrm{Re}(\hat{b}e^{i\omega_e t})$; the product of the factors a and b is

$$\begin{aligned}ab &= \mathrm{Re}(\hat{a}e^{i\omega_e t})\mathrm{Re}(\hat{b}e^{i\omega_e t}) = \mathrm{Re}[\hat{a}e^{i\omega_e t}\mathrm{Re}(\hat{b}e^{i\omega_e t})] \\ &= \mathrm{Re}\left[\hat{a}e^{i\omega_e t}\frac{1}{2}(\hat{b}e^{i\omega_e t} + \hat{b}^* e^{-i\omega_e t})\right] = \frac{1}{2}\mathrm{Re}\left(\hat{a}\hat{b}e^{2i\omega_e t} + \hat{a}\hat{b}^*\right)\end{aligned} \tag{8}$$

where the upper index * designates the complex conjugate. The first term oscillates harmonically at frequency $2\omega_e$; its time average is zero. Thus, the time average of ab is

$$\overline{ab} = \frac{1}{2}\mathrm{Re}(\hat{a}\hat{b}^*) \tag{9}$$

This formula is used to evaluate the time-average of a product of two first-order quantities. The time averages of terms A and B in Eq. (4) are thus evaluated as

$$\begin{aligned}\overline{A} &= \frac{1}{2}\mathrm{Re}(\hat{\boldsymbol{\alpha}} \times \hat{p}_1^*\underline{\mathbf{f}}) \\ \overline{B} &= \frac{1}{4}\mathrm{Re}[\hat{\boldsymbol{\alpha}} \times (\hat{\boldsymbol{\alpha}}^* \times p_0\underline{\mathbf{f}})]\end{aligned} \tag{10}$$

In order to determine the time average of $\underline{p}_2$ at the hull-fixed points in the term C in Eq. (4), terms containing third-order space derivatives of ϕ_0 are neglected, which yields the following result

$$\bar{C}=\frac{\rho\mathbf{f}_0}{2}\mathrm{Re}\Big[i\omega_e(\hat{\mathbf{a}}\times\hat{\mathbf{v}}_1^*)\nabla\phi_0-i\omega_e\nabla\hat{\phi}\hat{\mathbf{v}}_1^*+\frac{1}{2}[0,0,-g]^T(\hat{\boldsymbol{\alpha}}\times(\hat{\boldsymbol{\alpha}}^*\times\underline{\mathbf{x}}))$$
$$-\frac{1}{2}\left|\nabla\hat{\phi}-\nabla\phi_0\times\hat{\boldsymbol{\alpha}}\right|^2-(\nabla\phi_0-\mathbf{U})(-(\hat{\mathbf{v}}_1\nabla\nabla\phi_0)\times\hat{\boldsymbol{\alpha}}^*$$
$$+(\hat{\mathbf{v}}_1\times\hat{\boldsymbol{\alpha}}^*)\nabla\nabla\phi_0+\hat{\mathbf{v}}_1\nabla\nabla\hat{\phi}^*)\Big] \tag{11}$$

The time-averaged value of the remaining force contribution $\mathbf{F}_B$, caused by the varying hull submergence, is

$$\overline{\mathbf{F}_B}=\sum_{\text{WL panels}}\frac{|\hat{p}_w|^2}{4\rho g}\frac{\underline{\boldsymbol{\Delta}}_S\times(\underline{\mathbf{f}}\times\underline{\boldsymbol{\Delta}}_S)}{(\underline{\mathbf{f}}\times\underline{\boldsymbol{\Delta}}_S)_3} \tag{12}$$

where $\hat{p}_w$ is the amplitude of the pressure oscillation on the time-averaged waterline, $\hat{p}_w/(\rho g)$ is the linearized vertical relative motion between the water surface and hull, including swell-up, waterline (WL) panels are panels on the hull surface with two of their three corners located on the waterline, $\underline{\boldsymbol{\Delta}}_S$ is the vector between these corners, and index 3 designates the vertical component.

Second-order moments are calculated in a similar way.

Summing the longitudinal second-order force components yields the added resistance in head waves R_{aw}; the added resistance coefficient is defined as

$$C_{\text{aw}}=\frac{R_{\text{aw}}}{\rho g\zeta_a^2 B_{\text{wl}}^2/L_{\text{pp}}} \tag{13}$$

where B_{wl} is the ship's molded breadth and L_{pp} is its length between perpendiculars.

Numerical Performance

Both the steady nonlinear solution (the basis of the seakeeping solution) and the seakeeping solver use unstructured grids with triangular panels on the submerged body surface and block-structured grids with quadrilateral panels on the free surface. For symmetrical problems (symmetric body without lateral drift), only half of the body and free surface are discretized because the steady solution takes into account the symmetry condition, whereas radiation and diffraction problems in the seakeeping solver are separated into symmetrical and antisymmetrical parts. The same grid is used on the body, both for the steady and seakeeping problems; typically, about 2000 panels per half-body are employed. The grid and cell sizes on the free surface are automatically selected, depending on the ship size, its speed, and the direction and length of incoming waves; up to 20,000 panels can be used to discretize half of the free surface domain. The typical computational time is under one minute for one combination of incoming wave frequency and direction. To accelerate the computations, they can be performed for given encounter frequencies instead of given wave frequencies. If this is the case, about one minute is required for one encounter frequency for all specified wave directions. Further details of the numerical method, its implementation, and computational performance can be found in Ref. [26].

An important aspect was the calculation of the drift forces in short waves because applying Rankine source methods in short waves is computationally expensive. In longer waves, fine discretization of the ship hull surface and some minimum resolution of the free surface dominated the required computer memory and the computing time. With the increasing wave frequency of incoming waves, the required resolution of the free surface became dominant. Because the required number of panels in one direction increases in short waves inversely with the wave length (i.e., with the wave frequency squared), the total number of panels on the free surface in two directions increases proportionally to ω^4. Because direct solvers were used to solve the resulting linear equation system, the required computational time increased with the third power of the number of unknowns, i.e., approximately with ω^{12}. Such a steep increase in computational time limited the highest frequency that can be handled with Rankine source methods.

An alternative solution to calculate drift forces in short waves was used, based on the following consideration: because first-order ship motions in short waves are small, radiated waves do not need to be accurately resolved. When only an accurate resolution of diffraction waves and corresponding forces is required, in terms of the number of panels per wave length and number of wave lengths resolved in the solution domain, an accurate solution at acceptable computational memory is possible for waves longer than about one-tenth of the ship length, which is sufficient to predict drift forces in practically relevant irregular seaways.

Test Cases

Wigley III Hull. Although of little practical interest, the Wigley hull represents an interesting test case regarding added resistance in waves: large pitch motions due to its unconventional section form cause significantly greater added resistance than for usual hull forms.

Calculations were performed with GL Rankine for the Wigley III model with the midship section coefficient of 0.6667 at model scale; Table 1 lists the parameters of the tested model. Experiments [3] and RANS-based simulations [30] were used for comparison. In the experiments, the model was restrained in surge, whereas in the RANS simulations, several approaches to treat surge motion were tested and compared: (a) prescribed constant forward speed with restrained surge motions in waves, (b) towing with a constant forward speed of one end of a soft virtual spring, another end of which is attached to the model, and (c) free surge motion of the model with an imposed constant horizontal force modeling propeller thrust; these three numerical approaches showed marginal differences in the predicted added resistance in head waves.

KVLCC2 Tanker. The Maritime and Ocean Engineering Research Institute (MOERI) designed the KVLCC2 tanker. Table 2 lists the main particulars of the full-scale ship.

The GL Rankine code was used to calculate the added resistance in head waves for the full-scale ship at Froude numbers $\mathrm{Fr}=U/\sqrt{gL_{\text{pp}}}$ of 0.0, 0.05, 0.09, 0.142, and 0.18. Comparative model test measurements were available at scales of 1/58 and 1/100 [4,31].

Table 1 Main parameters of the Wigley III hull

L_{pp}	3.0 m
B_{wl}	0.3 m
T_{m}	0.1875 m
ϑ	0 deg
V	0.078 m^3
KG	0.170 m
k_{yy}	0.750 m

Table 2 Main particulars of the KVLCC2 tanker

L_{pp}	320.0 m
B_{wl}	58.0 m
T_{m}	20.8 m
ϑ	0 deg
V	3.126×10^5 m^3
KG	18.6 m
GM	5.710 m
k_{xx}	$0.4B_{\text{wl}}$
$k_{yy}=k_{zz}$	$0.25L_{\text{pp}}$

Table 3 Main particulars of the WILS containership

L_{pp}	321.0 m
B_{wl}	48.4 m
T_m	15.0 m
ϑ	0 deg
V	1.402×10^5 m^3
KG	21.296 m
GM	2.0 m
k_{xx}	19.073 m
$k_{yy} = k_{zz}$	77.228 m

WILS Containership. The containership, designed by the Maritime and Ocean Engineering Research Institute (MOERI), was model tested at a scale of 1/60 under the Joint Industry Project JIP WILS II [5]. Table 3 lists the main particulars of the full-scale ship. The GL Rankine code and the extended RANS solver COMET were used to compute added resistance in head waves for the full-scale ship at a Froude number of 0.183.

Two experimental techniques provided the average longitudinal force in waves. One technique relied on the sum of the spring forces; the other one on the relative surge displacement of the model with respect to the carriage. The resistance in calm water was subtracted from the post-processed resistance to obtain the added resistance in waves.

The RANS simulations [8] were performed on two different kinds of grids. Fine grids resolved the turbulent boundary layer and the steady ship wave system. Coarse grids were optimized to resolve incoming waves and wave-induced ship motions, but they did not accurately resolve the calm-water ship wave system and the calm-water resistance. On both kinds of grids, separate simulations obtained the calm-water resistance that was then subtracted from the average in the time value of the total resistance in waves, computed on the same grid, to obtain the value of the added resistance.

Results

Wigley III Hull. Figure 1 plots the GL Rankine-predicted heave amplitude (divided by the wave amplitude), pitch amplitude (divided by the wave slope amplitude), and coefficient C_{aw} of added resistance in waves (left, center, and right columns, respectively) for the Wigley III hull at Froude numbers of (top to bottom) 0.2, 0.3, and 0.4 compared with the RANS simulations [30] and experiments [3]; the horizontal axis shows the nondimensional wave frequency $\tilde{\omega} = (L_{pp}/\lambda_w)^{1/2}$.

At the two lower forward speeds (Fr = 0.2 and 0.3), the GL-Rankine-predicted motions and added resistance agree well with the experiments and RANS simulations, whereas at the largest forward speed (Fr = 0.4), GL Rankine overpredicts the measured and RANS-computed added resistance; the most important reason for the difference is nonlinearity. Due to the large pitch and heave motions, the amplitude of the absolute vertical motions at the bow is 13.0 cm in waves of amplitude 2.0 cm (used in the experiments), whereas the draft is only 19.0 cm. Thus, the hull

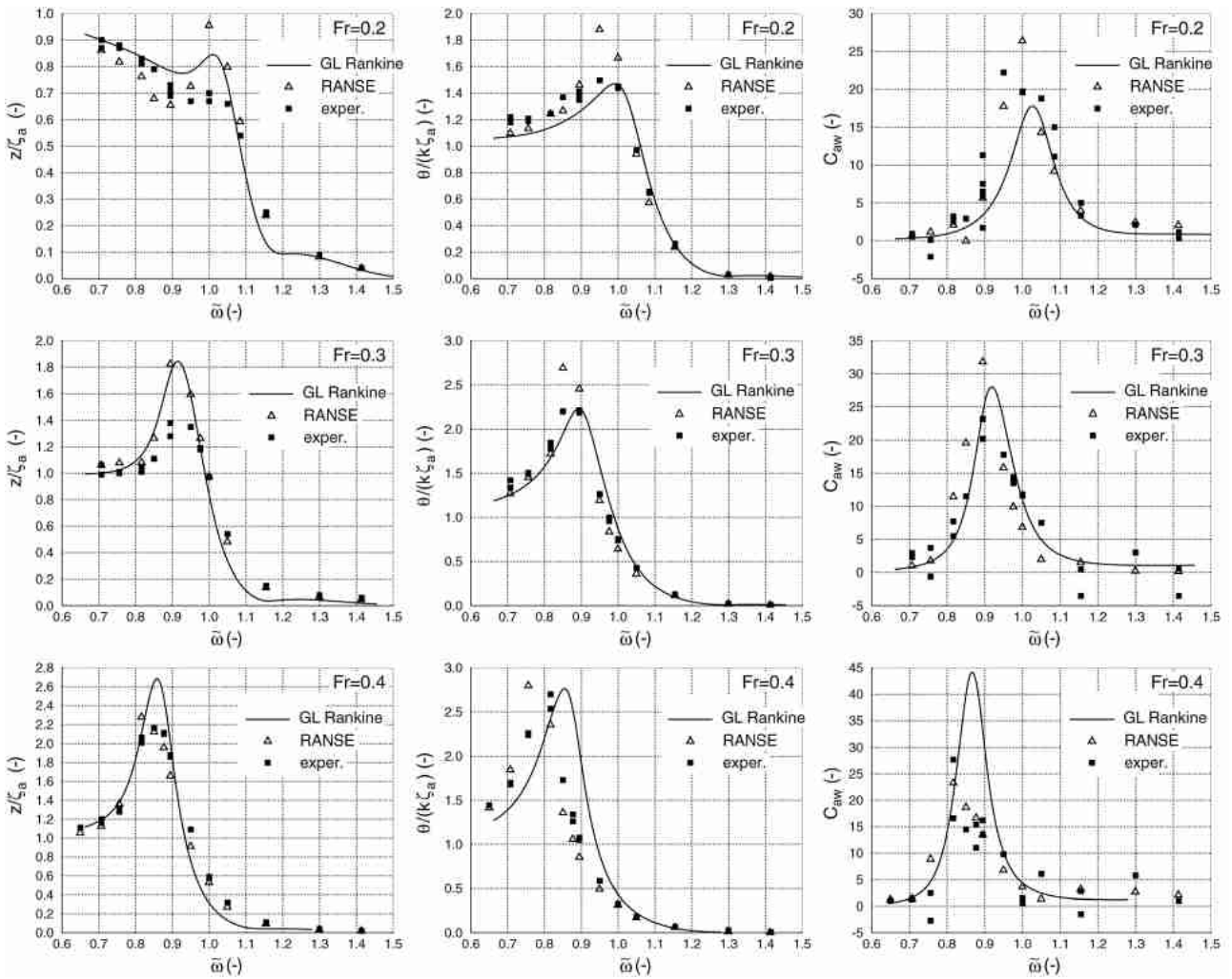

Fig. 1 Wigley III hull: GL Rankine predictions (—), RANS simulations in Ref. [30] (Δ), and experiments [3] (■)

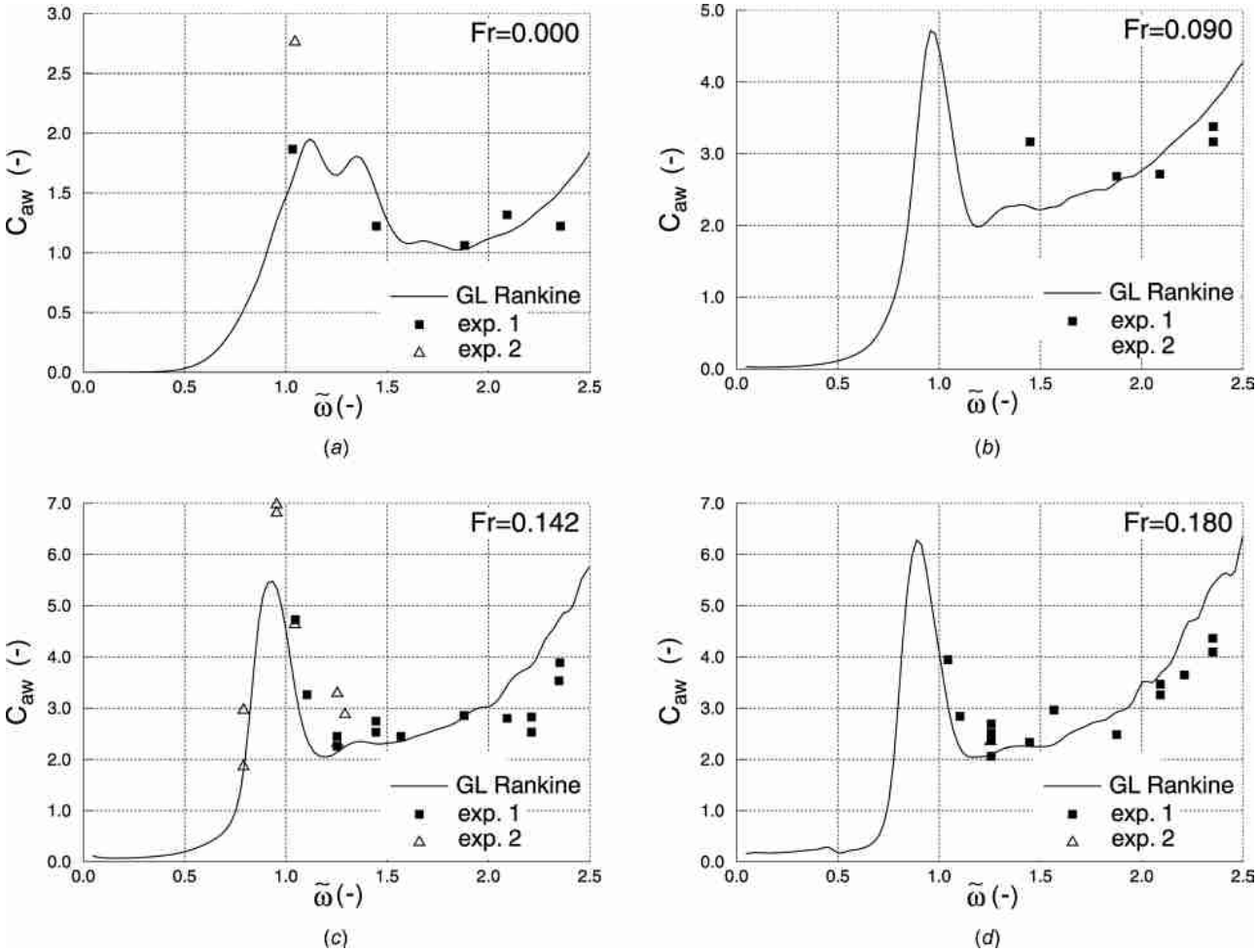

Fig. 2 KVLCC2 tanker: GL Rankine results (—) and experiments in Ref. [4] (■) and Ref. [31] (▲)

form above the still-water level, which was not considered by the GL Rankine method, should have a significant influence on the vertical motions and added resistance. Although, because of the very small model, viscous damping effects may also be relevant; they should have a smaller effect than the nonlinearity.

For the same model at Fr = 0.3, Ref. [19] reported over-prediction of the measured added resistance by their method, together with a shift of the added resistance peak to shorter waves compared to experiments. The authors attributed these effects to the under-estimation of the damping and to nonlinear effects and applied additional damping terms, derived from empirical viscous sectional lift and cross-flow drag coefficients, to reduce the added resistance peak.

KVLCC2 Tanker. Figure 2 plots the GL Rankine-predicted coefficient C_{aw} of the added resistance in waves as a function of the nondimensional wave frequency $\tilde{\omega}$ for the KVLCC2 tanker at Froude numbers of 0.0, 0.05, 0.09, 0.142, and 0.189, together with comparative model test measurements [4,31].

For this ship, the scatter of measured values is less than for the Wigley III hull. The large difference between the measurements [4,31] indicates the inherent difficulties associated with obtaining consistent measurements.

The GL Rankine code predictions compare favorably to measurements at all Froude numbers.

WILS Containership. Figure 3 plots the GL Rankine-predicted coefficients C_{aw} of the added resistance in waves as a function of the nondimensional wave frequency $\tilde{\omega}$ for the WILS containership at a Froude number of 0.189, together with the comparative model test measurements (top graph) and the results of the extended RANS solver COMET on fine and coarse grids (bottom graph). The difference between the two techniques to obtain the added resistance from the model tests is notable. This difference is especially significant in short (large $\tilde{\omega}$) waves.

The RANS predictions on the fine and coarse grids deviate from each other and this difference increases in short waves. It is unclear how close the fine grid values are to the converged results.

This situation again demonstrates the inherent difficulty in obtaining reliable estimates of added resistance, especially in

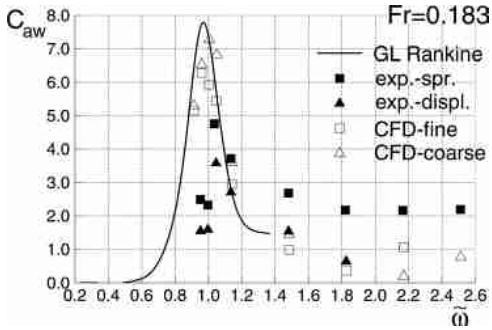

Fig. 3 WILS containership: GL Rankine results compared to measurements based on spring deformations (■) and model displacements (▲) and RANS predictions on fine (□) and coarse (Δ) grids

short waves. The GL Rankine code significantly over-predicts the measured values of added resistance, while it compares favorably with the RANS predictions.

Discussion

For the Wigley hull, GL Rankine predicts significantly larger added resistance in waves than for conventional hull forms (see Fig. 1). This was caused by the large pitch motions of this hull, brought about by its unconventional section shape. At higher Froude numbers, numerical predictions deviated significantly from the measurements, presumably due to nonlinear effects.

For the KVLCC2 tanker, the GL Rankine predictions compare well to measurements at all Froude numbers considered. The relatively large spread of measurements from different model tests is indicative of the inherent difficulties associated with obtaining consistent and reliable measurements that are suitable for a comparison to numerical predictions.

The containership was investigated at only one Froude number of 0.183. The two techniques used to obtain the model test data of the added resistance in waves show a considerable spread, demonstrating that it is problematic to achieve accurate measurements; see Fig. 3 (top). However, the GL Rankine predictions generally correlated favorably with the RANSE (Reynolds-averaged Navier-Stokes equations) solver results; see Fig. 3 (bottom). This demonstrated that the GL Rankine code was able to efficiently obtain reliable predictions of added resistance of ships in waves.

Conclusion

The Rankine panel method was used to predict the added resistance of three ship hulls in waves. Considering the difficulties associated with obtaining comparable model test data and their scatter, the predictions generally compared favorably with measurements. Although both the Rankine panel method and the RANS solver appear generally applicable, the potential flow method GL Rankine was appreciably faster than the RANS solver for the prediction of added resistance of ships in waves. Nevertheless, RANS-based simulations appeared suitable to provide reliable validation data for potential codes.

Nomenclature

$\mathbf{a}$ = vector expressed in inertial reference frame
$\hat{a}$ = complex amplitude of $a = \mathrm{Re}(\hat{a}e^{i\omega_e t})$
$\underline{\mathbf{a}}$ = vector expressed in body-fixed reference frame
B_{wl} = molded waterline breadth
C_{aw} = nondimensional coefficient of added resistance
C_B = block coefficient
Fr = Froude number
g = acceleration of gravity
GM = initial metacentric height
k_{xx}, k_{yy}, k_{zz} = radii of gyration
KG = center of gravity height above keel
L_{pp} = length between perpendiculars
$\mathbf{n}$ = normal vector
R_{aw} = added resistance in waves
T_{m} = draft amidships
$\mathbf{U}$ = relative water velocity due to forward ship speed $[-U, 0, 0]^T$
V = volume displacement
ζ_a = amplitude of a harmonic wave
λ_w = length of harmonic wave
v_{s} = ship speed
ρ = density of water
ϕ = first-order periodic perturbation potential
ϕ_0 = steady perturbation potential
ϕ^t = total potential
ω = wave frequency
ω_e = encounter frequency
$\tilde{\omega}$ = nondimensional wave frequency
ϑ = trim angle

References

[1] The Seakeeping Committee, 2008, "Final Report and Recommendations," Proceedings of the 25th ITTC, Vol. I, Fukuoka, Japan.
[2] Rathje, H., Schellin, T. E., and Brehm, A., 2011, "Speed Loss in Waves and Wave-Induced Torsion of a Wide-Breadth Containership," Proc. Inst. Mech. Eng., Part M: J. Eng. Marit. Environ., **225**(4), pp. 387–401.
[3] Journée, J. M. J., 1992, "Experiments and Calculations on 4 Wigley Hull Forms in Head Waves," Delft University of Technology, Report No. 0909.
[4] Bingjie, G., and Steen, S., 2010, "Added Resistance of a VLCC in Short Waves," ASME 29th International Conference on Ocean, Offshore and Arctic Engineering (OMAE 2010) Shanghai, China, June 6–11, pp. 609–617.
[5] Hong, S. Y., 2011, "Wave Induced Loads on Ships," Joint Industry Project II, MOERI, Report No. BSPIS503A-2207-2 (confidential).
[6] el Moctar, O., Oberhagemann, J., and Schellin, T. E., 2011, "Free Surface RANS Method for Hull Girder Springing and Whipping," Proceedings of the SNAME Annual Meeting, Houston, TX, Paper No. A56.
[7] Schellin, T. E., and el Moctar, O., 2007, "Numerical Prediction of Impact-Related Wave Loads on Ships," ASME J. Offshore Mech. Arct. Eng. **129**(1), pp. 39–47.
[8] Walter, S., 2011, "Analysis of an Approach to the Definition of the Added Resistance of Ships Due to Waves With RANSE Methods," Dipl. thesis, University of Duisburg-Essen (in German).
[9] Ley, J., Oberhagemann, J., el Moctar, B. O., Kaufmann, J., Shigunov, V., and Zorn, T., 2010, "Prediction of Ship Resistance and Ship Motions Using RANSE," Proceedings of the Gothenburg Workshop, Gothenburg, Sweden.
[10] Hirota, K., Matsumoto, K., Takagishi, K., Yamasaki, K., Orihara, H., and Yoshida, H., 2005, "Development of Bow Shape to Reduce the Added Resistance Due to Waves and Verification of Full Scale Measurement," Proceedings of the International Conference on Marine Research and Transportation, pp. 63–70.
[11] Kihara., H., Naito, S., and Sueyoshi, M., 2005, "Numerical Analysis of the Influence of Above-Water Bow Form on Added Resistance Using Nonlinear Slender Body Theory," J. Ship Res., **49**(3), pp. 191–206.
[12] Ström-Tejsen, J., Hugh, Y., Yeh, H., and Moran, D. D., 1973, "Added Resistance in Waves," Trans. Soc. Nav. Archit. Mar. Eng., **81**, pp. 109–143.
[13] Maruo, H., 1957, "The Excess Resistance of a Ship in Rough Seas," Int. Shipbuilding Prog., **4**(35), pp. 337–345.
[14] Maruo, H., 1960, "The Drift of a Body Floating on Waves," J. Ship Res., **4**(3), pp. 1–10.
[15] Maruo, H., 1963, "Resistance in Waves," J. Soc. Nav. Archit. Jpn., **8**, pp. 67–102.
[16] Joosen, W. P. A., 1966, "Added Resistance of Ships in Waves," Proceedings of the 6th Symposium on Naval Hydrodynamics, Washington, DC.
[17] Gerritsma, J., and Beukelman, W., 1972, "Analysis of Resistance Increase in Waves of a Fast Cargo Ship," Int. Shipbuilding Prog., **19**(217), pp. 285–293.
[18] Boese, P., 1970, "A Simple Method for the Calculation of Resistance Increase of a Ship in Seaway," J. Ship Technol. Res., **17**(86), pp. 1–15 (in German).
[19] Liu, S., Papanikolaou, A., and Zaraphonitis, G., 2011, "Prediction of Added Resistance of Ships in Waves," Ocean Eng., **38**(4), pp. 641–650.
[20] Faltinsen, O. M., Minsaas, K. J., Liapis, N., and Svein, S. O., 1980, "Prediction of Resistance and Propulsion of a Ship in a Seaway," Proceedings of the 13th Symposium on Naval Hydrodynamics, Tokyo, Japan, pp. 505–529.
[21] Bai, K. J., and Yeung, R. W., 1974, "Numerical Solutions to Free-Surface Flow Problems," Proceedings of the 10th Symposium on Naval Hydrodynamics, pp. 609–647.
[22] Joncquez, S. A. G., Bingham, H., and Andersen, P., 2008, "Validation of Added Resistance Computations by a Potential Flow Boundary Element Method," Proceedings of the 27th Symposium on Naval Hydrodynamics, Seoul, S. Korea.
[23] Kim, K.-H., and Kim, Y., 2010, "Numerical Analysis of Added Resistance of Ships," Proceedings of the 12th International Offshore and Polar Engineering Conference (ISOPE), Beijing, pp. 669–677.
[24] Bunnik, T. H. J., 1999, "Seakeeping Calculations for Ships, Taking Into Account the Non-Linear Steady Waves," Ph.D. thesis, Delft University of Technology.
[25] Söding, H., 2011, "Recent Progress in Potential Flow Calculations," Proceedings of the 1st International Symposium on Naval Architecture and Maritime, Istanbul, Turkey.
[26] Söding, H., von Graefe, A., el Moctar, O., and Shigunov, V., 2012, "Rankine Source Method for Seakeeping Predictions," ASME Proceedings of the 31st International Conference on Ocean, Offshore and Arctic Engineering (OMAE 2012), Rio de Janeiro, pp. 449–460.
[27] CD-adapco, 2002, "STAR-CD User Manual COMET, Version 2.0," CD-adapco, Nuremberg, Germany.
[28] CD-adapco, 2013, "User Manual Star-CCM+, Version 8.02.011," CD-adapco, Nuremberg, Germany.
[29] Hachmann, D., 1991, "Calculation of Pressures on a Ship's Hull in Waves," J. Ship Technol. Res., **38**, pp. 111–133.
[30] Ley, J., 2013, "Computations of Added Resistance and Motions of a Wigley Hull in Head Waves Using RANSE," Institute of Technology, Ocean Engineering and Transport Systems (ISMT), University of Duisburg-Essen, Germany.
[31] Gothenburg Workshop 2010, http://www.gothenburg2010.org/kvlcc2.html